Journal of
Drug Designing & Bioinformatics

JDDB, 1(1), 15-25, 2023
https://doi.org/10.58985/jddb.2023.v01i01.04
ISSN(Print):2959-3123

Research Article

Unraveling the molecular basis for GTP preference of unique histidine kinase BA2291 from *Bacillus anthracis* using a multilevel *in silico* approach

Mousumi Hazra* and **Ramesh Chandra Dubey**

Department of Botany and Microbiology, Gurukula Kangri (Deemed to be University), Haridwar- 249404, Uttarakhand, India

Article Information:
Received: 23 January, 2023
Revised: 15 February, 2023
Accepted: 18 February, 2023

Corresponding Author:
Mousumi Hazra
mousumi45@gmail.com;
mousumihazra.biotech@gmail.com
Phone: +91-8126915674

Academic Editor:
Prof. Dr. Samir Chtita

Keywords:
BA2291, *Bacillus anthracis*, anthrax, Molecular dynamics simulation, GTP, Histidine kinase.

Abstract

Enzyme histidine kinase (HK) is essential to a bacterial two-component system. Due to its exclusive presence in microorganisms, it is considered a critical antimicrobial target. The primary role of HK is to take part in transducing signals in an NTP-dependent manner. As a phosphoryl donor HK family popularly uses Adenosine Triphosphate (ATP). Enzyme BA2291 from *Bacillus anthracis* is a rare exception that uses Guanosine Triphosphate (GTP). BA2291 is a part of the sporulation mechanism of *B. anthracis*. Sporulation regulates the transformation between the vegetative and spore-forming phases. Therefore, BA2291 plays an essential role in the survival of *B. anthracis*, making the protein a unique and exciting target for a novel antibacterial hunt. Utilizing the interdisciplinary *in silico* methods of Predictive Modeling, Docking, and Molecular Dynamics (MD), the present communication unravels the biochemical evidence behind its preference for GTP over ATP. Anthrax is a well-known life-threatening disease. However, this disease has yet to be wholly eradicated anthrax due to the deficiency of our understanding. The present study would be instrumental in unraveling the molecular basis for HK functioning and developing a platform for designing anti-anthrax therapeutics.

1. Introduction

Multidrug resistance (MDR) is the most concerning and growing problem nowadays. The emergence of such MDR bacteria urges a severe need for novel antibiotics with entirely new and innovative mechanisms of action. Today's advancement in modern biological research leads to the characterization of many novel pathways in bacteria, which could serve as a novel target. Two-component system [1], which comprises histidine kinase and a response regulator [2], is widespread in bacteria and plays a crucial role in signal transduction, especially in stress conditions. As mammals undergo different signal transduction pathways and don't possess histidine kinases as their essential proteins, they could serve as a potential target for antimicrobial agents.

A phosphorelay pathway regulates the transition between the vegetative cycle and sporulation in *B. anthracis*. This phosphorelay pathway is similar to *Bacillus subtilis* [3], where Spo0A plays a central part in sporulation signal transduction. Several histidine kinases are involved in the regulation of the level of Spo0A phosphorylation. In the case of *B. subtilis*, a very extensively studied model organism, five sensor histidine kinases (Kin A, B, C, D, E) take part in this pathway [4]. In *B. anthracis*, the path is even more complicated. There are nine genes, including putative sporulation histidine kinases. Those HKs were identified based on the identity and similarity of genes compared with HisKA domain of *B. subtilis*. Chromosomally

encoded protein BA2291 was recognized as significant sporulation kinase belonging to *B. anthracis* [5]. The specialty of BA2291 in *B. anthracis* is that it exclusively utilizes GTP, not ATP, for being auto-phosphorylated. This is considered a unique and rare example among the histidine kinases.

Domain in histidine kinases that takes part in auto catalysis comprises the conserved motifs known as H, N, G1, F, and G2 boxes for binding ATP nucleotide. BA2291 has high conservation in sequence in this region but significantly differs in G1. The typical sequence motif in histidine kinase is DxGxG, whereas the sequence completely changes in BA2291. The sequence in BA2291 is NNGPM; Asn and Met, respectively, replace the two striking differences, Asp and fifth Gly. In general, the G1 box plays a critical role in ATP binding; structural studies on histidine kinase (HK583) of *Thermotoga maritima* showed the formation of a hydrogen bond between one of the carbonyl oxygen atoms of the Asp and amine of the Adenine group. Structural modeling on the same site for GTP suggests that the oxygen of GTP at position O6 forms a comparable hydrogen bond with the NH_2 group of Asn, followed by an additional hydrogen bond formed between the amine group of guanine and the backbone 'N' of Met. This suggests that the GTP binding domain of BA2291 is structurally analogous to the ATP binding domain of the other histidine kinases. But, the presence of Asn at this position in the motif of BA2291, called the G1 box, prefersto bind to GTP instead of ATP [6].

In the current study, interdisciplinary *in silico* methods have been applied to BA2291 using the enzyme's structural and dynamic features to understand the molecular reason causing the alteration in the preference of phosphorylation agent from ATP to GTP. This study shows the difference in the mode of binding of two nucleotides and favoring GTP over ATP [7].

2. Materials and Methods

2.1. Homology modeling

Homology modeling or comparative structural modeling of a protein refers to the building up of a three -dimensional atomic resolution model of the target protein. This is based on the primary sequence of the target protein and an experimental three-dimensional structure of a structurally and functionally related protein called a 'template.'

The method of homology modeling is divided into the following steps. The first step includes searching for several comparable sequences to single out an ideal template that could represent a homologous protein of BA2291 structurally and functionally. An online software, BLAST available from NCBI [8] was used to perform a protein alignment search. The sequences retrieved from the above-mentioned operation were submitted into the Multalin program for multiple sequence alignment in the second step [9]. In the third step, the sequence homology of BA2291 was at most 15%, which needs to be improved to develop a good quality model. *Geobacillus stearothermophilus* KinB (GsKinB), a histidine kinase (PDB ID 3D36) [10], shows more than 30% identity to BA2291 catalytic domain enabled the development of the predictive model of BA2291 catalytic domain. In the fourth step, the SWISS-MODEL server was used for predictive modeling with the GskinB structure as a template [11]. Further, to work on the amino acid residues from the BA2291 enzyme's core catalytic region, other programs COOT [12] and SWISS PDB Viewer were used [13]. The predicted model was also validated for phi-psi torsional angles from Ramachandran plot using the PDBSUM [14, 15].

The above-mentioned model was further improved by energy minimization using the GROMACS software package [16]. After performing 5000 steps of energy minimization by steepest descent method, the MD simulation for 300 ps was carried out to examine the quality of the model structures and check their stability.

After the optimization procedure, the validity of the structure was verified by comparing the compatibility of the amino acid sequence of a known 3D structure of protein. Finally, the stereo-chemical quality of the model was checked using PROCHECK method [17].

2.2. Molecular docking

The software AutoDockVina 1.2 is used to carry out the molecular docking experiment for the current study [18]. After a thorough docking calculation, Autodock Vina aims to determine the best possible pose of a ligand bound to a protein utilizing its global search algorithm. The 3D structures of the ligands (ATP and GTP) were retrieved from the PDB extracting two unrelated co-crystal structures containing ATP as a ligand [19, 20]. The AutoDock tool (ADT) [21] has been thoroughly used to build up the protein, ligand

structure, and docking protocol. The developed homology model of BA2291 was used as the receptor in a rigid mode. Every polar hydrogen present in the system was assigned, every non-polar hydrogen was merged, and ultimately the PDBQT files were developed by adding charges to the receptor and the ligands. For the ligand, to define all possible torsions of the bonds that are rotatable, the AutoTors utility of ADT was utilized. Determination of a grid map considering the active receptor site was done using the dimension of 20 × 18 × 22 points and grid center of -4.0 × -1.0 × 90.0, and spacing of 1.0Å between the grid points. Each docking operation was performed to generate ten docking conformations of every ligand. For further proceedings, the binding affinity of the ligands was screened, and conformations with the highest binding affinity were considered.

2.3. MD simulation

Software package GROMACS was used to perform all molecular dynamics (MD) simulations of the apo and binary complexes [16, 22] utilizing the GROMOS96 force field 54A7 [23]. The starting structures for the 100 ns simulations (total of 300 ns simulation) of the BA2291 apo, BA2291-GTP, and BA2291-ATP complexes were obtained from the homology modeling and molecular docking of ATP and GTP to the catalytic domain of BA2291, respectively (described above). Dundee PRODRG Server [24] was used for generating the topology of the GTP and ATP molecules. The partial atomic charges of GTP and ATP were calculated using CHelpG [25] method incorporated in Gaussian03 [26, 27] program at the level of b3lyp/6-31(g). Each system (BA2291 apo, BA2291-GTP, and BA2291-ATP) was placed in the center of a box with dimensions 8.0 × 8.0 × 8.0 nm. The box contained approximately ~16320 water molecules with simple point charge (SPC) for three systems. A few water molecules were replaced to buffer the system by adding positively charged sodium ions.

After that, energy minimization of all three neutralized systems was performed using the steepest descent method for 3000 steps. 200ps of position-restrained simulations were applied to these structures. The protein and the ligands were kept fixed, and water molecules were allowed to settle around the protein-ligand complex. These structures were finally used for the aqueous solution's final MD simulations. NPT ensemble was used to carry out those simulations. The SETTLE algorithm [28] was used to constrain the bond length and angle of the water molecules. The LINCS algorithm [29, 30] was used to restrain the bond length of the peptides. The Particle Mesh Ewald (PME) method was used to evaluate the long-range electrostatic interactions [31]. A constant pressure of 1 bar was applied with a coupling constant of 1.0 ps; peptide, water molecules, and ions were coupled separately to a bath at 300 K with a coupling constant of 0.1 ps. The PBC was applied, and the equation of motion was integrated at time steps of 2 fs. The analysis tools available in the GROMACS program package [22] have been utilized to analyze the different MD trajectories [32, 33]. A clustering algorithm was carried out to the MD trajectory of the BA2291-GTP and BA2291-ATP complex for cluster analysis [34]. The VMD suite [35, 36] and PyMol [37] were also extensively used to analyze and prepare structural diagrams. The fastDRH web server [38] was also used to calculate the binding free energy between the ATP and BA2291 based on automated molecular docking and MM-PBSA/GBSA computation. This server utilizes the following equation to predict the ligand-protein interaction energy.

$$\Delta G = \alpha V_{VdW} + \beta V_{Elec} + \gamma V_{H\text{-}bond} + \delta V_{M\text{-}bond} + \varepsilon \Delta G_{Sol} + \phi \Delta G_{Entropy} + \eta$$

V_{VdW}, V_{Elec}, $V_{H\text{-}bond}$, and $V_{M\text{-}bond}$ represent the Van der Waals interaction, electrostatic interaction, hydrogen bonding interaction, and interaction energy with metals, respectively. ΔG_{sol} and $\Delta G_{Entropy}$ represent solvation-free energy change due to ligand binding and a change in conformational entropy in the ligand binding process, respectively. The coefficients α, β, γ, δ, ε, ϕ and η are the scaling parameters obtained from multiple regression analysis to fit the experimental data with the computed binding free energies. Fifty snapshots were saved at regular intervals to calculate the average interaction energy. Chimera [39] was used for interaction studies and making high-quality videos from simulation trajectories.

3. Results and Discussion

3.1. Homology modeling

There are 377 amino acids in the enzyme BA2291. Multiple domains are observed while performing sequence analysis and alignment of BA2291 with known proteins from GenBank. Unfortunately, even with the closest homolog of 1 full-length BA2291, the sequence homology of the template is less than 16%, with the closest structural homolog. But there are 150 amino acids containing the catalytic domain of BA2291. According to a local sequence-based alignment search, 27% identity between the GsKinB and BA2291 catalytic

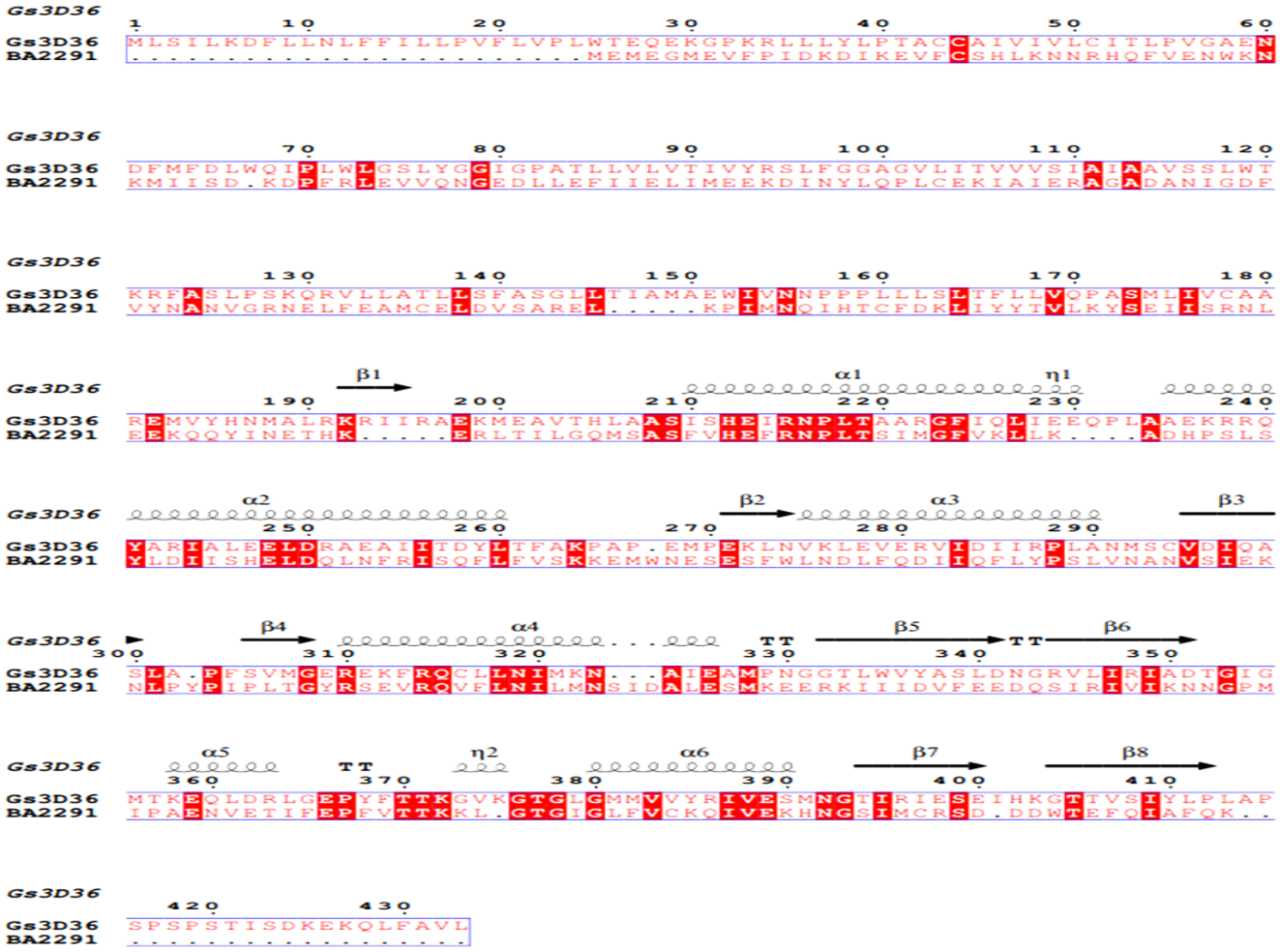

Figure 1. Sequence alignment of 3D36 and BA2291 sequence for finding similarity and identity.

domain (amino acid residues 234-376) was recorded. According to the literature report, GsKinB also belongs to the HK family, confirming its choice as a very well-suited template. Finally, the 3D structure of GsKinB from PDB ID 3D36 was used as a template to develop the predictive homology model. (Fig. 1).

The primary rough model was further refined by applying the energy minimization process, and the optimized structure is finalized and shown in Fig. 2. In the final model, we found 4 essential alpha helices and five beta sheets which are a critical part of the structure associated with connecting loops and turns.

In structural comparisons with other related proteins, the presence of G1-Box, G2-Box, F-Box, and N-Boxes was identified, which are hallmark regions of a histidine kinase. The structure shown here represents the model's

lowest energy conformation, which was compared by superimposing with the structure of GsKinB. The structural alignment was measured using a root means

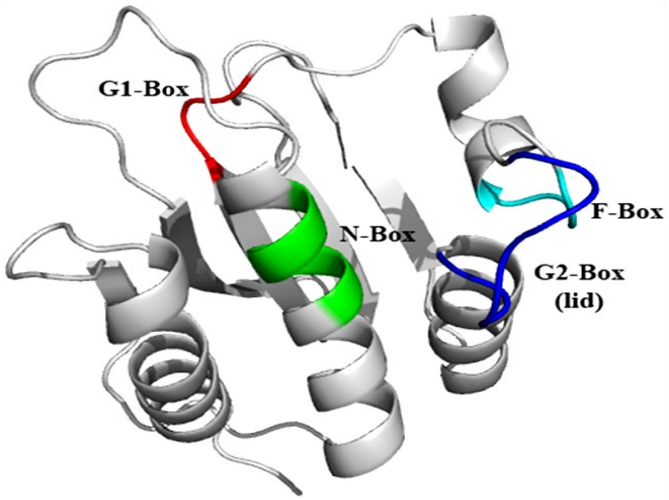

Figure 2. Homology model of BA2291.

square deviation (RMSD) method and the evaluated value is 1.0Å, which indicates an excellent alignment of the model with the template.

The quality check of the final structure was performed using the software PROCHECK. From the analysis, it

was observed that various critical factors like stereo-chemical positioning, energetic distribution, and packing environment were entirely in agreement with the template. In addition, evaluation of the main and side chain conformations, presence of rotamers, average lengths of the bonds, and contacts between residues are very much within the standard criteria. The statistics based on the Ramachandran plot show that the majority (85.9%) of residues are in the most favored region, only 10.9% of residues are obtained in the additional allowed regions, and only the rest (2.3%) the residues are in generously allowed regions. More interestingly, among the total of 150 residues, only Thr201 was found in the disallowed part of the plot (Fig. 3). All those statistics summarize the existence of a model one can rely on.

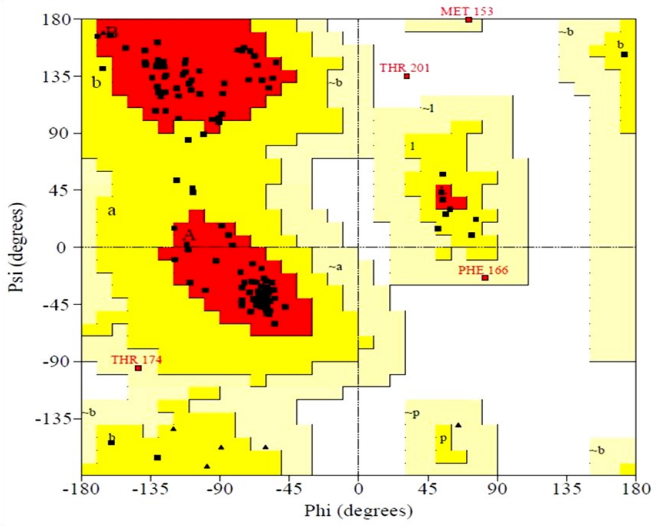

		No. of residues	%-tage
Most favoured regions	[A,B,L]	110	85.9%
Additional allowed regions	[a,b,l,p]	14	10.9%
Generously allowed regions	[~a,~b,~l,~p]	3	2.3%
Disallowed regions	[XX]	1	0.8%
Non-glycine and non-proline residues		128	100.0%
End-residues (excl. Gly and Pro)		2	
Glycine residues		6	
Proline residues		7	
Total number of residues		143	

Figure 3. Ramachandran plot of BA2291.

3.2. Molecular docking

Docking was performed with the software AutodockVina using a standard protocol with the unbound 3D structure of the template (PDB ID: 3D36) and ligand ADP. Interestingly, ADP present in 3D36 and an entirely different structure were used in parallel to remove the biases of the initial conformation. The validation results show that AutodockVina can accurately reproduce the crystal pose of ADP with 0.5Å deviation (Fig. S1).

To obtain a starting point for the MD simulation optimized structure of enzyme BA2291 was used in docking studies with two NTPs, ATP and GTP. Fig. S2 shows the docked positions of ATP and GTP within the active site of BA2291. Docking studies with the modeled BA2291 catalytic domain provided insight into activity differences of very similar structures. ATP and GTP are structurally very similar. Both of them consist of triphosphorylated deoxyribose sugar and a purine base. Their only difference is the difference in the functional groups on the base moiety, which differ in their hydrogen bonding pattern in DNA.

3.3. Molecular dynamics simulations of BA2291 with GTP and ATP

In this present study, the interaction of GTP and ATP with BA2291 has been investigated. In particular, three independent MD simulations of BA2291-GTP and BA2291-ATP complexes and BA2291 apo structures have been carried out in an aqueous environment with an explicit water model. The well-accepted strategy to monitor the equilibration of a system is to investigate the root-mean-square deviation (RMSD).

The RMSD of the Cα atoms of the two trajectories, BA2291-GTP and BA2291-ATP complexes and BA2291 apo structures, are plotted (Fig. S3). This plot indicates that all the systems attain equilibrium. As the system reached equilibrium, the trajectories were used for further analysis.

3.3.1. Interaction between GTP with BA2291

Several nonbonding interactions play critical and essential roles in macromolecules and ligand-protein interactions. The coulombic and van der Waals (vdW) interaction energy between the GTP molecule and the BA2291 is plotted against time.

The time evolution of coulombic interaction shows that the average interaction energy between GTP and BA2291 is -292.9 kJ/mol (Fig. 4a), whereas the vdW interaction between GTP and BA2291 is -83.0 kJ/mol (Fig. 4b). Another significant nonbonding interaction is hydrogen bonding. The hydrogen bonds between GTP and BA2291 were calculated. The distance cutoff between the donor and acceptor was set to 0.35 nm, and the angle cutoff between the acceptor, donor, and hydrogen was set to 30o. The plot of the number of

hydrogen bonds with time indicates that the average number of hydrogen bonds formed by GTP with the CA domain of the BA2291 is around 7 (Fig. 5). The inter-atomic distance between the atoms from BA2291 and GTP that form the hydrogen bond is given in Table 1. The most representative structure obtained from the MD simulation shows that the GTP molecule interacts with the Asn286, Asp289, Asn317, Met321, Thr336, Thr337, Lys338, Thr342, and Thr369 residues within the CA domain of BA2291 (Fig. 6a). These interactions can be divided into three regions depending on the conserved boxes. The purine base interacts with the residues from the G1 box of the CA domain. The sugar ring interacts with the N box, and the phosphate groups

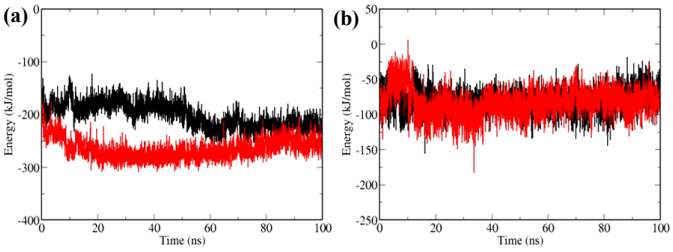

Figure 4. (a) Coulombic interaction between GTP (red) and ATP (black). **(b)** van der Waals interaction between GTP (red) and ATP

interact with N and G2 boxes.

The time-dependent plot of the distance between the OG1 atom of Thr369 of BA2291 and the thN1 atom of GTP shows a strong interaction and continues for the

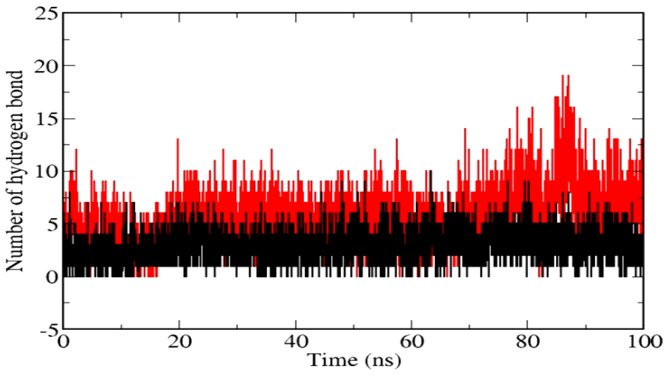

Figure 5. Number of hydrogen bond formed by BA2291 with GTP (red) and ATP (black).

rest of the simulation (Fig. 7a). On the other hand, the distance between the side chain atoms (ND2 and OD1) of Asn317 and N1 of GTP is maintained steadily throughout the simulation.

These results indicate that the purine base of GTP interacts strongly with the side chain of Thr369 and Asn317. The N2 atom is also responsible for making a strong hydrogen bond with the backbone O of Met321

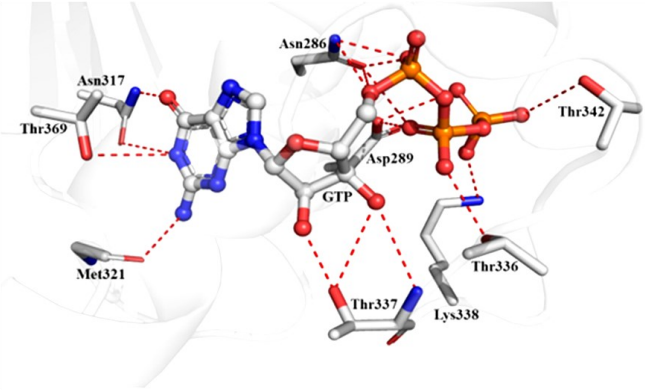

Figure 6. (a) Interaction between the residue from BA2291 and GTP.

located at the G1 box. The critical observation is the orientation of the ribose sugar at the binding site.

The O5* atom of the ribose ring orients toward the N box of the BA2291 and strongly interacts with the side chain ND2 and OD1 traces of Asn286 residue from the N box. This orientation of the ribose sugar is different from the observed co-crystal structures of other ADP-bound histidine kinases. But, closer scrutiny of the NMR -derived structures of the CA domain of histidine kinases shows that a similar kind of orientation of ADP is also possible where the oxygen atom of the ribose ring orients towards the N box of a histidine kinase [40]. The O2* atom of the ribose ring interacts with the OG1 atom of Thr337, whereas the O3* atom of GTP makes a hydrogen bond with the major chain N and side chain OG1 atoms of Thr337.

The phosphate group of GTP interacts strongly with the side chain of Asn286. The β phosphate group is stabilized by the side chains of Asn286, Asp289, and Thr336, whereas the P-O bond of the γ phosphate is stabilized by the strong hydrogen bonding interaction with the side chain of Asp289, Lys338, and Thr342 (Fig. 6a).

To calculate the interaction energy between protein and ligand, the fastDRH web server was used. The average interaction energy between GTP and BA2291 was estimated at -43.62±0.35 kcal/mol.

Understanding protein-substrate interaction charge-based interactions played an extremely critical role. From the calculation of the charge-based protein-ligand interaction map of the BA2291-GTP complex, a comparable positive charge distribution is observed

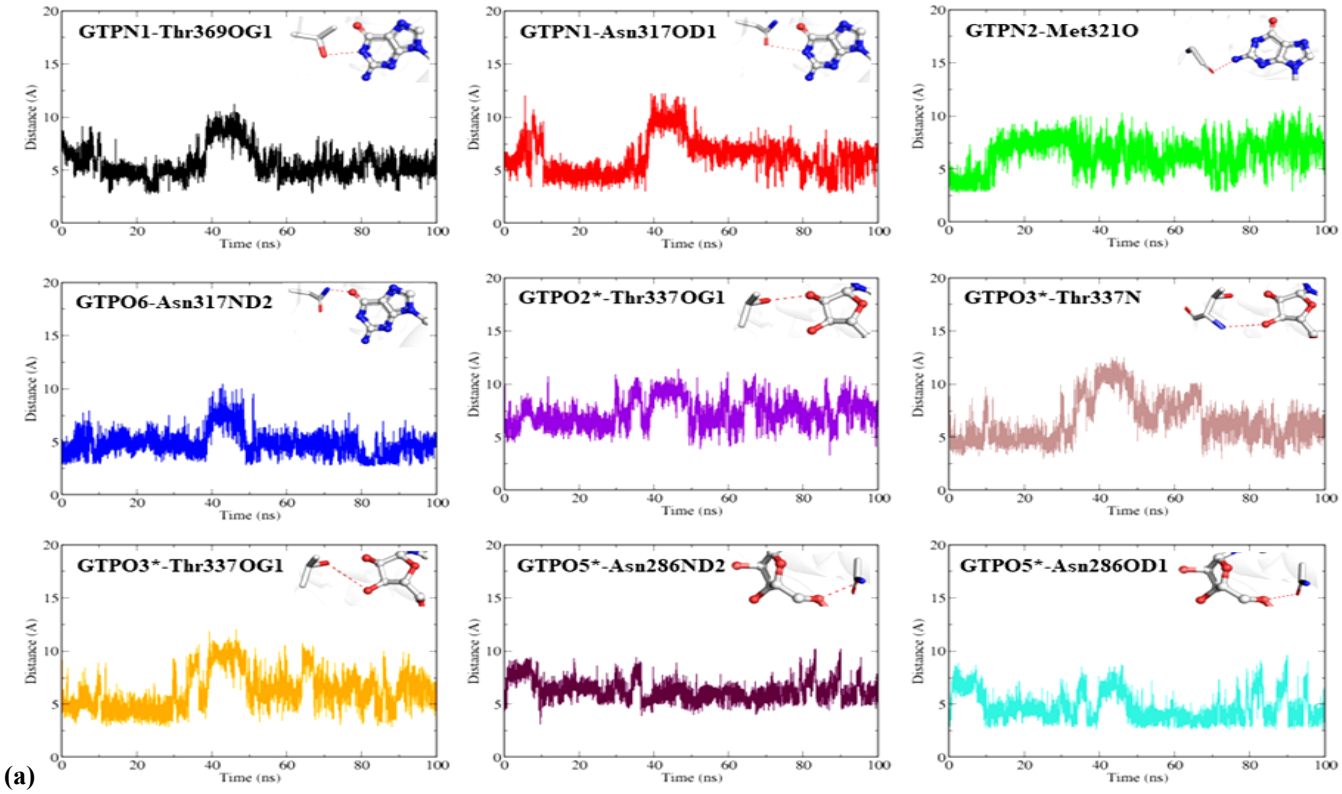

Figure 7. (a) Distance measurement between interacting atoms of amino acid residues of BA2291 with GTP.

around the O_6 atom of GTP (Fig. 8a). The imidazole nucleus of the purine ring orients toward the negatively charged residue. From the result, it could be concluded that electrostatic interaction is extremely important for

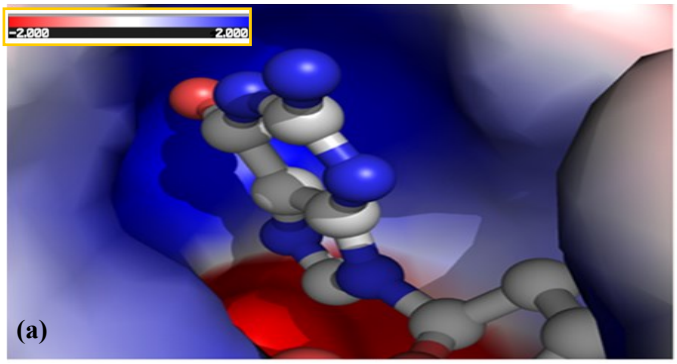

Figure 8. (a) The electrostatic potential (kT/e) mapped on the surface of BA2291 and the interacting mode of GTP.

adequately positioning the GTP molecule in the enzyme's active site.

3.3.2. Interaction between ATP with BA2291

The plot of the coulombic interaction between ATP and BA2291 shows the average interaction energy -190.9 kJ/mol (Fig. 4a), which is around 102 kJ/mol lower than the coulombic interaction between GTP and BA2291. At the same time, the average VdW interaction energy between

Table 1. Interactions of ATP and GTP with BA2291.

ATP	Protein (BA2291)		Distance (Å)	GTP	Protein (BA2291)		Distance (Å)
	Residue	Atom Name			Residue	Atom Name	
N6	Asn317	ND2	3.4	N1	Thr369	OG1	3.3
N6	Asn286	O	2.8	N1	Asn317	OD1	3.4
O2*	Thr337	OG1	2.7	N2	Met321	O	3.1
O2*	Thr337	N	3.1	O6	Asn317	ND2	2.4
O3*	Thr337	N	2.6	O2*	Thr337	OG1	2.6
O3*	Thr336	OG1	2.9	O3*	Thr337	N	3.5
				O3*	Thr337	OG1	3.5
				O5*	Asn286	ND2	2.8
				O5*	Asn286	OD1	3.5
O1A	Asn286	ND2	2.8	O1A	Asn286	ND2	2.6
O1A	Asn286	OD1	3.0	O1A	Asn286	OD1	2.3
O1B	Lys338	NZ	3.1	O1B	Thr336	OG1	3.0
O2B	Thr336	OG1	2.3	O2B	Asn286	OD1	3.1
O2G	Thr342	OG1	3.3	O2B	Asp289	OD2	3.2
				O1G	Thr342	OG1	3.5
				O2G	Lys338	NZ	2.8
				O3G	Asp289	OD2	3.4

ATP and BA2291 throughout the trajectory was observed to be -81.0 kJ/mol (Fig. 4b). This value is almost equal to the value obtained for the GTP BA2291. This result indicates that GTP and BA2291 are mainly governed by strong electrostatic interaction, whereas the vdW interaction plays a similar role for GTP and ATP.

The number of hydrogen bonds formed by ATP with BA2291 is around 4, which is twice less than the number of hydrogen bonds formed by GTP with BA2291 (Fig. 5). The hydrogen bonding distance between the atoms from BA2291 and ATP is given in Table 1. Structures from MD simulation reveal that the residues Asn286, Asp317, Thr336, Thr337, Lys338, and Thr342 of BA2291

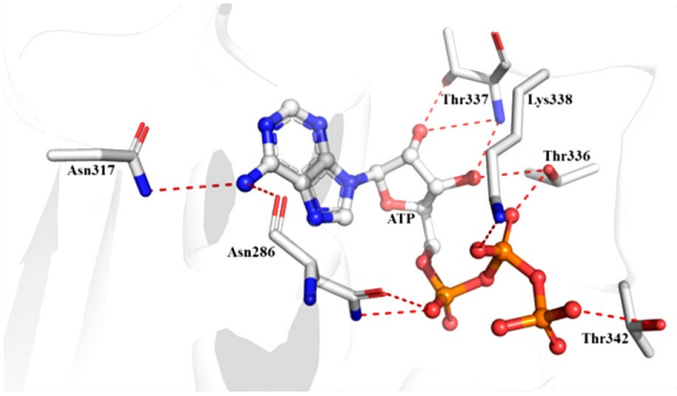

Figure. 6: (b) Interaction between the residue from BA2291 and ATP.

interact with ATP (Fig. 6b).

Similar to the GTP, the interacting regions of ATP can also be divided into three regions. The purine base of ATP interacts with the G1 box, the ribose sugar interacts with the N box, and phosphate groups interact with the N and G2 boxes of BA2291. Asn317, Met321, and Thr369 of BA2291 are responsible for solid interaction with GTP's purine base. But in the case of ATP, the distance between the N6 atom of ATP and the ND2 atom of Asn317 and between the N6 atom of ATP and peptide O of Asn286 were measured. The time-dependent plot of these two distances suggests that the strong interaction with Asn317 and Thr369 that was present with GTP has been wholly lost in the presence of ATP. The N6 atom of ATP only interacts moderately with the backbone O of Asn286. The O2* and O3* atoms of ribose sugar of ATP interact with OG1 and N atoms of Thr337, whereas the O3* atom only makes hydrogen bond interaction with the OG1 atom of Thr336. The α phosphate group interacts strongly with the side chain of Asn286. The β phosphate group is stabilized with OG1 atom of Thr336 and NZ atom of Lys338. The γ phosphate group makes a strong hydrogen bonding interaction with the side chain OG1 atom of Thr342 (Fig. 7b).

The interaction energy between the ATP and BA2291 was calculated to be -38.56 ± 0.37 kcal/mol, which is around 5 kcal/mol lower than the calculated binding energy between GTP and BA2291. This result suggests that BA2291 has a slightly higher preference for GTP than ATP. The electrostatic potential calculated for BA2291 in presence of ATP shows the unfavorable interaction at the adenine binding site (Fig. 8b). The higher positive charge densities around the purine base of ATP could be one of the critical factors that destabilize ATP binding. Moreover, compared to GTP, the electrostatic potential map at the nucleotide-binding site of BA2291 is unfavorable for ATP.

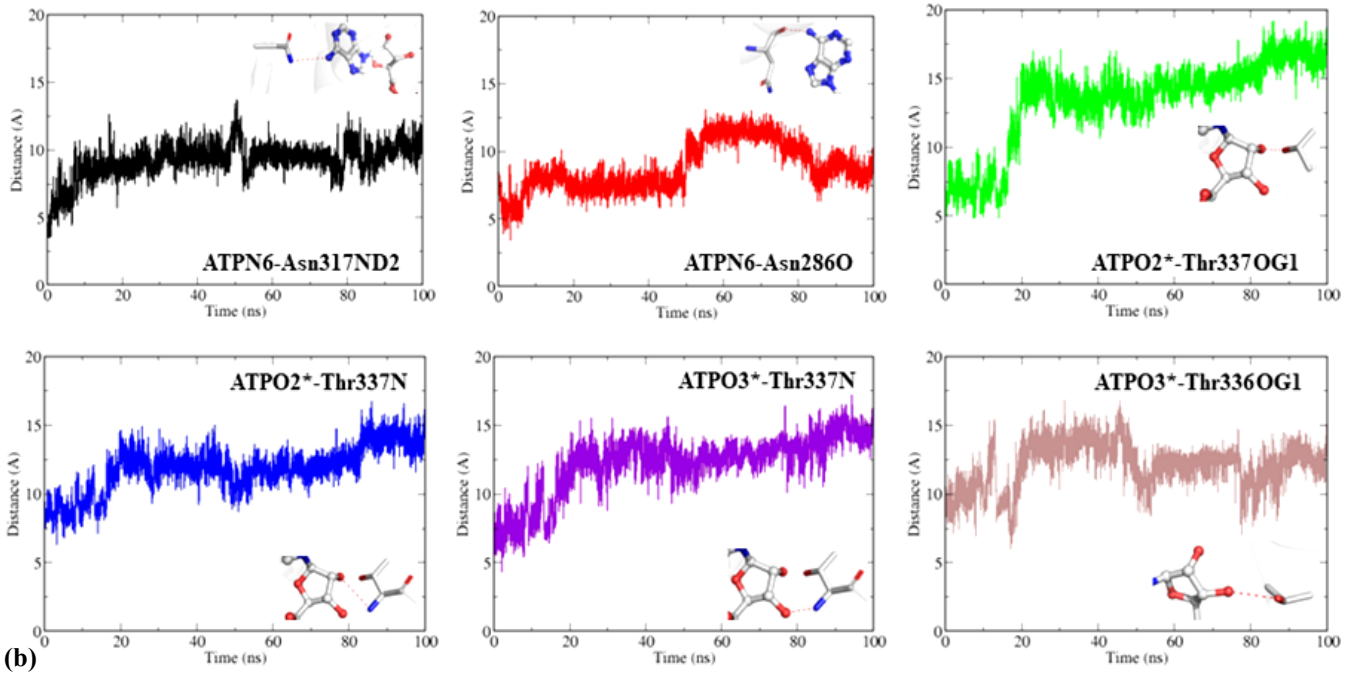

Figure 7. (b) Distance measurement between interacting atoms of amino acid residues of BA2291 with ATP.

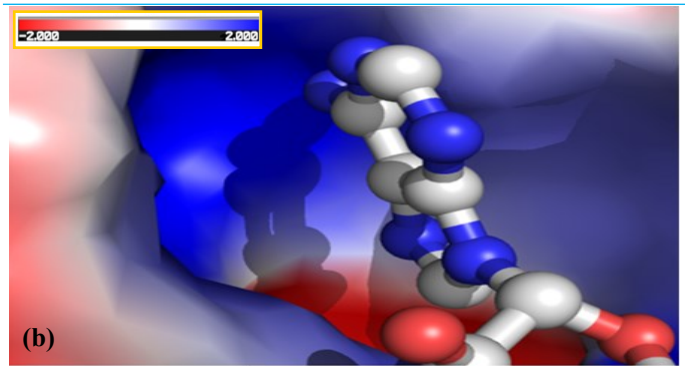

Figure 8. (b) The electrostatic potential (kT/e) mapped on the surface of BA2291 and the interacting mode of ATP.

4. Conclusion

In the current study, homology modeling was used to create the molecular model of the catalytic domain of protein BA2291. Using this modeled structure, *in silico* methods like docking studies and molecular dynamics simulation were performed to understand the uniqueness of BA2291, as a GTP binder. We have analyzed factors such as backbone RMSD, number of H-bonds, length of H-bonds, coulombic and van der Waals interaction, and interaction energy. The above results imply that the interaction of GTP with BA2291 is stronger and more stable than ATP. These undoubtedly provide a molecular-level explanation of BA2291's preference for GTP over ATP as an auto-phosphorylating agent. Protein BA2291 is a histidine kinase that plays a crucial role in the sporulation of *Bacillus anthracis*. With the emergence of antibacterialdrug resistance, histidine kinases are becoming a potential antimicrobial target. Our study would contribute more information towards the fundamental biochemical way of histidine kinases work. Furthermore, this study would also create the possibility of designing potential therapeutics against the life-threatening disease anthrax.

Supplementary data

Supplementary Figure S1
Supplementary Figure S2
Supplementary Figure S3

Authors' contributions

MH: Conceptualization; Data curation; Formal analysis; Investigation; Methodology; Software; Validation; Visualization; Roles/Writing-original draft preparation. RCD: Supervision; Writing-review & editing.

Acknowledgments

The authors thank the Head of the Department of Botany and Microbiology, Gurukula Kangri (Deemed to be University), for providing a computer facility. We wish to thank the other institutions for helping to conduct a part of the work, namely ICC (IIT-Roorkee), Bioinformatics Facility, Department of Biosciences and Bioengineering (IIT-Roorkee), for the provision of computational facilities and support.

Funding

This research did not receive any specific grant from funding agencies in the public, commercial, or not-for-profit sectors.

Conflicts of Interest

The authors declare no conflict of interest.

References

1. Stock, A. M.; Robinson, V. L.; Goudreau, P. N. Two-Component Signal Transduction. Annu. Rev. Biochem. 2000, 69, 183-215.
2. West, A. H.; Stock, A. M. Histidine Kinases and Response Regulator Proteins in Two-Component Signaling Systems. Trends Biochem. Sci. 2001, 26, 369-376.
3. White, A. K.; Hoch, J. A.; Grynberg, M.; Godzik, A.; Perego, M. Sensor Domains Encoded in Bacillus Anthracis Virulence Plasmids Prevent Sporulation by Hijacking a Sporulation Sensor Histidine Kinase. J. Bacteriol. 2006, 188, 6354-6360.
4. Read, T. D.; Peterson, S. N.; Tourasse, N.; Baillie, L. W.; Paulsen, I. T.; Nelson, K. E.; Tettelin, H.; Fouts, D. E.; Eisen, J. A.; Gill, S. R.; et al. The Genome Sequence of Bacillus Anthracis Ames and Comparison to Closely Related Bacteria. Nature. 2003, 423, 81-86.
5. Stranzl, G. R.; Santelli, E.; Bankston, L. A.; La Clair, C.; Bobkov, A.; Schwarzenbacher, R.; Godzik, A.; Perego, M.; Grynberg, M.; Liddington, R. C. Structural Insights into Inhibition of Bacillus Anthracis Sporulation by a Novel Class of Non-Heme Globin Sensor Domains. J. Biol. Chem. 2011, 286, 8448-8458.
6. Scaramozzino, F.; White, A.; Perego, M.; Hoch, J. A. A Unique GTP-Dependent Sporulation Sensor Histidine Kinase in Bacillus Anthracis. J. Bacteriol. 2009, 191, 687-692.
7. Tzeng, Y. L. A Unique Sensor Histidine Kinase. J. Bacteriol. 2009, 191, 681-682.
8. Altschul, S. F.; Gish, W.; Miller, W.; Myers, E. W.; Lipman, D. J. Basic Local Alignment Search Tool. J. Mol. Biol. 1990, 215, 403-410.
9. Corpet, F. Multiple Sequence Alignment with Hierarchical Clustering. Nucleic Acids Res. 1988, 16, 10881-10890.
10. Bick, M. J.; Lamour, V.; Rajashankar, K. R.; Gordiyenko, Y.; Robinson, C. V.; Darst, S. A. How to switch off a

histidine kinase: crystal structure of Geobacillus stearothermophilus KinB with the inhibitor Sda. J. Mol. Biol. 2009, 386, 163-177.

11. Arnold, K.; Bordoli, L.; Kopp, J.; Schwede, T. The Swiss-Model Workspace: A Web-Based Environment for Protein Structure Homology Modelling. Bioinformatics. 2005, 22, 195-201.
12. Emsley, P.; Cowtan, K. Coot: Model-Building Tools for Molecular Graphics. Acta Crystallogr., Sect. D: Biol. Crystallogr. 2004, 60, 2126-2132.
13. Guex, N.; Peitsch, M. C. Swiss-Model and the Swiss-PDB Viewer: An Environment for Comparative Protein Modeling. Electrophoresis. 1997, 18, 2714-2723.
14. Laskowski, R. A.; Hutchinson, E. G.; Michie, A. D.; Wallace, A. C.; Jones, M. L.; Thornton, J. M. PDBsum: A Web-Based Database of Summaries and Analyses of All PDB Structures. Trends Biochem. Sci. 1997, 22, 488-490.
15. Laskowski, R. A. PDBsum New Things. Nucleic Acids Res. 2009, 37, D355-D359.
16. Van Der Spoel, D.; Lindahl, E.; Hess, B.; Groenhof, G.; Mark, A. E.; Berendsen, H. J. Gromacs: Fast, Flexible, and Free. J. Comput. Chem. 2005, 26, 1701-1718.
17. Laskowski, R. A.; MacArthur, M. W.; Moss, D. S.; Thornton, J. M. Procheck: A Program to Check the Stereochemical Quality of Protein Structures. J. Appl. Crystallogr. 1993, 26, 283-291.
18. Trott, O.; Olson, A. J. Autodock Vina: Improving the Speed and Accuracy of Docking with a New Scoring Function, Efficient Optimization, and Multithreading. J. Comput. Chem. 2010, 31, 455-461.
19. Hazra, S.; Konrad, M.; Lavie, A. The Sugar Ring of the Nucleoside Is Required for Productive Substrate Positioning in the Active Site of Human Deoxycytidine Kinase (DCK): Implications for the Development of DCK-Activated Acyclic Guanine Analogues. J. Med. Chem. 2010, 53, 5792-5800.
20. Sabini, E.; Hazra, S.; Konrad, M.; Lavie, A. Elucidation of Different Binding Modes of Purine Nucleosides to Human Deoxycytidine Kinase. J. Med. Chem. 2008, 51, 4219-4225.
21. Morris, A. L.; MacArthur, M. W.; Hutchinson, E. G.; Thornton, J. M. Stereochemical Quality of Protein Structure Coordinates. Proteins: Struct., Funct., Bioinf. 1992, 12, 345-364.
22. Hess, B.; Kutzner, C.; van der Spoel, D.; Lindahl, E. Gromacs 4: Algorithms for Highly Efficient, Load-Balanced, and Scalable Molecular Simulation. J. Chem. Theory Comput. 2008, 4, 435-447.
23. Schuler, L. D.; Daura, X.; van Gunsteren, W. F. An Improved GROMOS96 Force Field for Aliphatic Hydrocarbons in the Condensed Phase. J. Comput. Chem. 2001, 22, 1205-1218.
24. Schüttelkopf, A. W.; van Aalten, D. M. Prodrg: A Tool for High-Throughput Crystallography of Protein–Ligand Complexes. Acta Crystallogr., Sect. D: Biol. Crystallogr. 2004, 60, 1355-1363.
25. Breneman, C. M.; Wiberg, K. B. Determining Atom-Centered Monopoles from Molecular Electrostatic Potentials. the Need for High Sampling Density in Formamide Conformational Analysis. J. Comput. Chem. 1990, 11, 361-373.
26. Hehre, W. J.; Lathan, W. A.; Ditchfield, R.; Newton, M. D.; Pople, J. A. GAUSSIAN 70, Program No. 236, Quantum Chemistry Program Exchange. Indiana University, Bloomington, IN. 1973.
27. Pople, J. A.; Head-Gordon, M.; Fox, D. J.; Raghavachari, K.; Curtiss, L. A. Gaussian-1 Theory: A General Procedure for Prediction of Molecular Energies. J. Chem. Phys. 1989, 90, 5622-5629.
28. Miyamoto, S.; Kollman, P. A. Settle: An Analytical Version of the Shake and Rattle Algorithm for Rigid Water Models. J. Comput. Chem. 1992, 13, 952-962.
29. Hess, B.; Bekker, H.; Berendsen, H. J.; Fraaije, J. G. Lincs: A Linear Constraint Solver for Molecular Simulations. J. Comput. Chem. 1997, 18, 1463-1472.
30. Bandekar, D.; Mohapatra, S.; Hazra, M.; Hazra, S.; Biswas, S. N-Terminal Truncation of VC0395_0300 Protein from Vibrio Cholerae Does Not Lead to Loss of Diguanylate Cyclase Activity. Biophys. Chem. 2021, 268, 106493.
31. Darden, T.; Perera, L.; Li, L.; Pedersen, L. New Tricks for Modelers from the Crystallography Toolkit: The Particle Mesh Ewald Algorithm and Its Use in Nucleic Acid Simulations. Structure. 1999, 7, R55-R60.
32. Paul, M.; Hazra, M.; Barman, A.; Hazra, S. Comparative Molecular Dynamics Simulation Studies for Determining Factors Contributing to the Thermostability of Chemotaxis Protein "Chey." J. Biomol. Struct. Dyn. 2013, 32, 928-949.
33. Hazra, M.; Dubey, R. C. In Silico Study of Cox Protein from P2 Type Enteric Bacteriophages Based on Sequence, Structure and Dynamics to Understand Its Functional Integrity. J. Biomol. Struct. Dyn. 2021, 40, 14035-14050.
34. Hazra, M.; Dubey, R. C. Interdisciplinary in Silico Studies to Understand In-Depth Molecular Level Mechanism of Drug Resistance Involving NS3-4A Protease of HCV. J. Biomol. Struct. Dyn. 2022, 1-20 (published online).
35. Humphrey, W.; Dalke, A.; Schulten, K. VMD: Visual Molecular Dynamics. J. Mol. Graph. 1996, 14, 33-38.
36. Hsin, J.; Arkhipov, A.; Yin, Y.; Stone, J. E.; Schulten, K. Using VMD: An Introductory Tutorial. Curr. Protoc. Bioinform. 2008, 24, 5-7.
37. DeLano, W. L. The PyMOL molecular graphics system. DeLano Scientific, San Carlos, CA, USA. http://www.

pymol. org. 2002.

38. Wang, Z.; Pan, H.; Sun, H.; Kang, Y.; Liu, H.; Cao, D.; Hou, T. fastDRH: A Webserver to Predict and Analyze Protein–Ligand Complexes Based on Molecular Docking and MM/PB(Gb)SA Computation. Brief. Bioinform. 2022, 23, bbac201.
39. Pettersen, E. F.; Goddard, T. D.; Huang, C. C.; Couch, G. S.; Greenblatt, D. M.; Meng, E. C.; Ferrin, T. E. UCSF Chimera?a Visualization System for Exploratory Research and Analysis. J. Comput. Chem. 2004, 25, 1605-1612.
40. Tanaka, T.; Saha, S. K.; Tomomori, C.; Ishima, R.; Liu, D.; Tong, K. I.; Park, H.; Dutta, R.; Qin, L.; Swindells, M. B.; et al. NMR Structure of the Histidine Kinase Domain of the E. Coli Osmosensor EnvZ. Nature, 1999, 396, 88-92.